Studies of DNA- and HSA-binding properties of new nano-scale green synthesized Ni (II) complex as anticancer agent using spectroscopic methods, viscosity measurement, molecular docking, MD simulation and QM/MM

Monireh Dehkhodaei, Mehdi Sahihi, Hadi Amiri Rudbari, Sajjad Gharaghani, Reza Azadbakht, Salman Taheri, Abolghasem Abbasi Kajani

Studies of DNA- and HSA-binding properties of new nano-scale green synthesized Ni (II) complex as anticancer agent using spectroscopic methods, viscosity measurement, molecular docking, MD simulation and QM/MM

Monireh Dehkhodaei [a], Mehdi Sahihi [a], Hadi Amiri Rudbari [a], Sajjad Gharaghani [b], Reza Azadbakht [c], Salman Taheri [d], Abolghasem Abbasi Kajani [a]

[a] Department of Chemistry, University of Isfahan, Isfahan 81746-73441, Iran

[b] Department of Bioinformatics, Laboratory of Chemoinformatic, Institute of Biochemistry and Biophysics, University of Tehran, Tehran, Iran

[c] Department of Chemistry, Payame Noor University, P.O. Box 19395-3697, Iran

[d] Chemistry and Chemical Engineering Research Center of Iran, Tehran, Iran

Abstract

Herein, we synthesized a new nano-scale Schiff base Ni(II) complex in water as a green solvent and at ambient temperature. The compound was characterized using FT-IR and elemental analysis. Also, its molecular structure was determined by single crystal X-ray diffraction technique. The MTT assay results indicated that the anticancer activity of the compound is affected by its size. Finally, binding ability of the nano-scale Ni(II) Schiff base complex with calf thymus DNA and human serum albumin was investigated using combination of experimental (UV–Vis, fluorescence, circular dichroism (CD) and viscosity) and computational (molecular docking, molecular dynamics simulation and qm/mm) methods. The estimated binding constants for the DNA-complex and HSA-complex were about 10^4 M^{-1}. Molecular docking studies revealed the binding of Ni(II) complex to the minor groove of DNA and warfarin binding site of protein by formation of hydrogen bond, π-cation and hydrophobic interactions. MD simulation studies revealed that complexation with NiL_2 changed the structure of HSA when compared to free protein. Finally, the ONIOM results showed that the structural parameters of the compound changed along with binding to DNA and HSA, indicating the strong interaction between the compound and these biomacromolecules.

Keywords

Binding

Nano complex

MTT assay

Molecular docking

MD simulation

ONIOM

1. Introduction

More than 40% of compounds with pharmacological activity that are introduced as drugs have poor water solubility problem. Beside, reducing the size of drugs to nano-scale causes the several unique properties that could not be seen in their bulk form; including high surface to volume ratio, unique magnetic behavior and adjusting of their dispersibility in various solvents [1]. Hence, synthesis of nano-scale drugs has attracted many researchers due to the abovementioned properties [2], [3], [4]. Schiff base compounds are considered as a very important class of organic materials, due to their interesting chemical and physical properties [5]. The Schiff base ligands have high coordination capability and many strong biological properties. Although these compounds have been extensively studied, they are still highly regarded [6]. Schiff base ligands exhibited the biological activity such as antitumor, antibiotics, antifungal, antimicrobial, and anticancer properties [7], [8], [9], [10]. Also, they have appropriate affinity for binding to HSA and DNA [11], [12], [13]. The azomethine linkage in Schiff bases is responsible for their biological activity and several studies proved that the presence of lone pair electrons in sp^2-hybridized orbital of nitrogen atom of the azomethine group plays a remarkable chemical and biological role. On the other hand, the metal ions present in complexes, not only accelerate the drug activity of compounds, but also increase the effectiveness and efficiency of the ligands [14], [15]. Hence, great effort has been devoted to design and development of Schiff base complexes using different metal ions, which possess excellent antioxidant, antibacterial and antitumor activities. Nickel plays a role in urease as a member of redox enzymes family [16], [17]. Also, considerable biological activities are reported for Ni(II) Schiff base complexes [12], [18]. It is clear that many compounds utilize their drug effects through binding to DNA or carrier proteins such as Human Serum Albumin (HSA). Studying on the interactions of these metal complexes with DNA or HSA is critical to design target specific, more efficient and less toxic drugs. Interaction of candidate drugs with these biomacromolecules could be reflected using spectroscopic (fluorescence, UV–Vis and so on) and computational methods (molecular docking, molecular dynamics simulation and qm/mm).

Recently, we have focused on designing and synthesis of novel Schiff base ligands, and investigation of their assembly with metals as well as their biological activities [11], [12], [13]. Herein, a new Schiff base Ni(II) complex (NiL_2) was synthesized in water as a green solvent and at ambient temperature. These conditions are valuable to introduce a compound as a drug candidate. Then the compound was characterized using FT-IR and elemental analysis. In addition, its molecular structure was determined by single crystal X-ray diffraction technique. The cell viability percent of HeLa cancer cells was first studied by MTT assay. In order to increase the colloidal stability and suitability for the biomedical applications, the nano-scale compound was also synthesized and used for in vitro studies. Finally, binding ability of the nano-scale Ni(II) Schiff base complex with calf thymus DNA (CT-DNA) and HSA was investigated using combination of experimental (UV–Vis, fluorescence, circular dichroism (CD) and viscosity) and computational (molecular docking, molecular dynamics simulation and qm/mm) methods.

2. Experimental section

2.1. Materials sources

All of the used chemicals for synthesis of the complex including 3-amino-prop-1-ene (Allylamine), 2-hydroxybenzaldehyde (salicylaldehyde), triethylamine and nickel acetate ($Ni(OAc)_2$) were purchased from Merck Co. and were used without further purification. All of the used salts for buffer preparation were analytical grade and were dissolved in double distilled water. All of the solutions were used freshly after preparation. Also, human serum albumin (HSA), CT-DNA, RPMI-1640 medium, Fetal bovine serum (FBS), dimethyl sulfoxide (DMSO), antibiotics (penicillin-streptomycin) solution, and 3-(4,5-dimethylthiazol-2-yl)-2,5-diphenyltetrazolium bromide (MTT) were obtained from Sigma-Aldrich.

2.2. Synthesis of the bulk and nano-scale Ni (II) Schiff base complex (NiL_2)

The solution (5 ml) of Allylamine (IUPAC name: 3-amino-prop-1-ene) (4 mmol) in double distilled water was added slowly to 5 ml of a methanolic stirred solution of salicylaldehyde (IUPAC name: 2-hydroxybenzaldehyde) (4 mmol) in ambient temperature. The color immediately changed to yellow and the mixture was then stirred for 2 h before removal of solvent under vacuum. A solution of triethylamine (4 ml) in double distilled water was added dropwise to ligand solution. The mixture was stirred for 15 min again. Then, a solution of appropriate metal salt ($Ni(OAc)_2$ (2 mmol)) in absolute deionized water (60 ml) was added to the mixture, gently, for synthesis of the complex in bulk. The resulting solution was stirred for 1 h in room temperature. After concentration, dark green precipitate was collected by filtration and was washed with methanol and deionized water several times. Appropriate single crystals for X-ray crystallography were obtained directly from the reaction mixture. In order to prepare the complex in nano-scale; ultrasonic probe was fixed in ligand solution and was positioned under the high-intensity ultrasonic waves. At this time, a solution of $Ni(OAc)_2$ (2 mmol) in 60 ml deionized water was added to the mixture gently under ultrasonic condition for 2 h. The green powder was isolated from the solution and was purified by washing with methanol and deionized water several times and was allowed to get dried at room temperature.

2.3. Single crystal diffraction studies

X-ray data for NiL_2 were collected on a STOE IPDS-II diffractometer with graphite monochromated Mo-Kα radiation. For NiL_2, a green crystal was chosen using a polarizing microscope and was mounted on a glass fiber which was used for data collection. Data were collected at temperature of 298 K in a series of [1] scans in 1° oscillations and were integrated using the Stöe X-AREA [19] software package. A numerical absorption correction was applied using the X-RED [20] and X-SHAPE [21] softwares. The data were corrected for Lorentz and Polarizing effects. The structure was solved by direct methods using SIR2004 [22]. The non-hydrogen atoms were refined anisotropically by the full-matrix least-squares method on F^2 using SHELXL [23]. All hydrogen atoms were added at ideal positions and were constrained to ride on their parent atoms.

2.4. Cell viability assay

The potential anticancer activities of the bulk solution and nano-scale NiL_2 dispersion were studied using MTT assay on human breast cancer cell line ((MCF-7)) according to the previously reported

procedure [24]. Briefly, the cancer cells were first cultured in RPMI-1640 medium supplemented with 10% FBS and 1% antibiotics solution and were maintained in a humidified 5% CO_2 incubator at 37 °C for two weeks. After propagation of the cells and obtaining the appropriate density, the cells were harvested and were seeded on 96-well plates at a density of 104 cells per well containing 200 µl medium. The cells were subsequently incubated overnight at the same conditions before treatment with different concentrations (10, 20, 50 and 100 µM) of the bulk and nano-scale NiL_2 complex for 48 h. The medium was then removed and 100 µl MTT solution (0.5 mg/ml in media) was added into each well and the plates were incubated again at 37 °C for 4 h. Finally, the medium was carefully discarded and the remained formazan crystals were dissolved in 150 µl DMSO and the absorbance was measured at 570 nm. Three independent experiments were conducted for each toxicity endpoint and the results were presented as the mean values obtained from three independent experiments. The cell viability was determined as ratio of absorbance values from each treatment and the control. To further evaluate the anticancer effects of the compounds, the cell morphology changes after exposure to the compounds were also monitored by optical microscope.

2.5. Preparation of DNA, HSA and nano-scale NiL_2 for binding experiments

The stock solution of CT-DNA was prepared in 50 mM Tris buffer at pH 7.5 using double-distilled deionized water and was stored at 4 °C. The CT-DNA concentration per nucleotide was determined using absorption intensity at 260 nm after adequate dilution with the buffer and using the reported molar absorptivity of 6600 $M^{-1}\cdot cm^{-1}$ [25]. Purity of CT-DNA solution was confirmed by ratio of UV absorbance at 260 and 280 nm (A260/A280 = 1.9), indicating that CT-DNA is free from protein impurity [26]. Also, a stock solution of HSA was prepared by dissolving the desired amount of HSA in 50 mM phosphate buffer (pH = 7). The HSA stock solution was stored at 4 °C in the dark and was used within 2 h. HSA concentration was determined by UV–Vis spectrophotometry using the molar absorption coefficient 35,700 $M^{-1}\cdot cm^{-1}$ at 278 nm [27]. The appropriate amount of the nano-scale NiL_2 was dispersed in Tris and phosphate buffer for DNA and HSA binding experiments, respectively.

2.6. Fluorescence spectroscopy measurements

Fluorescence quenching experiments were carried out using quartz cuvette with 1 cm optical path length and the excitation and emission slits were set at 5 and 10 nm, respectively. In our primary experiments, ethidium bromide (EB) emission was checked in the presence of various amounts of CT-DNA. The results showed that the emission of EB was increased up to mole ratio of CT-DNA:EB = 10:1 and there was no significant increasing in emission after the mentioned mole ratio. Hence, the CT-DNA solution was stirred with EB with molar ratio of CT-DNA:EB 10:1 and was incubated for 1 h at 4 °C for completion of interaction between CT-DNA and EB. Then, various amounts of nano-scale NiL_2 dispersion (250 µM) were added to the mixture of CT-DNA:EB. The fluorescence spectra were measured in the range of 500–700 nm with exciting wavelength at 520 nm. In each measurement after addition of NiL_2, the mixture was allowed to stand for 2 min. Moreover, the measured fluorescence intensities were corrected for the dilution and the inner-filter effect. To eliminate the inner filter effects, absorption measurements were carried out at the fluorescence excitation and emission wavelengths. The extent of this effect can be roughly evaluated with the following relationship: [28]

$$F_{corr} = F_{obs} \times e^{(Aex+Aem)/2} \quad (1)$$

where, F_{corr} and F_{obs} are the corrected and observed fluorescence intensities, respectively, and A_{ex} and A_{em} are the absorption of NiL_2 at excitation and emission wavelengths, respectively. All the fluorescence intensities obtained in this study were corrected. For investigation of the HSA interaction with NiL_2 by this technique 2 ml of HSA solution (10 μM) was placed into the quartz cell and various amounts of NiL_2 (200 μM) were added to the cell. The fluorescence intensities were measured with excitation wavelength at 295 nm and emission wavelength range of 300–450 nm. In each measurement, the mixture was allowed to incubate for 2 min after addition of the complex. Furthermore, all intensities were corrected for the dilution and inner filter effect in fluorescence experiments.

2.7. UV–Vis absorption spectroscopy measurements

Absorption spectroscopy titration experiment was performed by addition of various amounts of CT-DNA (1 mM) to 2 ml of nano-scale NiL_2 dispersion (200 μM). All NiL_2–CT-DNA solutions were allowed to incubate for 2 min before recording the related spectra. Absorption curves of NiL_2–CT-DNA mixtures were corrected by subtracting the spectra of CT-DNA and all intensities were corrected for the dilution effect. The UV–Vis absorption spectra of HSA solution (10 μM) in the absence and presence of various amounts of the nano-scale NiL_2 dispersion (200 μM) were recorded after 2 min of incubation. All intensities were corrected for the dilution effect.

2.8. Circular dichroism spectroscopy

The circular dichroism (CD) spectra were recorded at room temperature using 0.1 cm quartz cell in the far-UV region (200–260 nm) for HSA and in the far and near-UV (205–310) for DNA to clarify the structural changes of biomacromolecules during their interaction with NiL_2. The CD spectrum of HSA and DNA solution was recorded before and after addition of the nano-scale NiL_2 complex with molar ratio of 1:1.

2.9. Viscosity measurement

Viscosity experiments were carried out using a rotational viscometer and the measurements were performed at 200 rpm at room temperature. The viscosity of CT-DNA solution was measured in the presence of various amounts of the nano-scale NiL_2 dispersion. The obtained data are presented as $(\eta/\eta^0)^{1/3}$ versus [NiL_2] / [CT-DNA], where η and η^0 are the viscosity of CT-DNA in the absence and presence of NiL_2, respectively.

3. Computational section

3.1. Molecular docking calculations

Docking study was carried out to indicate the HSA and DNA-binding site for NiL_2 complex. The 3D structure of NiL_2 was obtained using the .cif file of its X-ray crystal structure. The .cif file was converted to the .pdb format using the Mercury software (http://www.ccdc.cam.ac.uk/). The crystal structures of HSA (PDB ID: 1AO6) and DNA (PDB ID: 423D) with sequence $d(ACCGACGTCGGT)_2$ were taken from the Brookhaven Protein Data Bank (http://www.rcsb.org/pdb). The resolution of these files was 2. 5 and 1.6 Å for HSA and DNA,

respectively. Water molecules of the .pdb files were deleted, missing hydrogen atoms and Gasteiger charges were added. Flexible ligand docking was carried out by AutoDock 4.2.5.1 molecular docking program using the implemented empirical free energy function and the Lamarckian Genetic Algorithm [29]. The Gasteiger charges were added to prepare the macromolecule input file for docking and the AutoGrid was used to calculate grids. For docking of the NiL_2 complex to HSA the grid box was centred on C_α of the Trp-214 residue of protein and a docking with 90 lattice points along X, Y, and Z axes was performed to find the active site of complex to the HSA. Grid point spacing was set to 0.375 Å, to allow the complex to rotate freely. For the docking of NiL_2 complex with DNA, a blind docking with 126 lattice points along X, Y, and Z axes was performed to find the binding site of complex on DNA with a grid point spacing of 0.375 Å, to allow the complex to rotate freely. In the next step, the centre of the grid box was located at the binding site and the second docking was performed using a cubic box with 90 × 90 × 90 dimensions. 250 docking runs with 25,000,000 energy evaluations for all runs were performed.

3.2. Molecular dynamics (MD) simulation

MD simulation method was used to compare the structural changes of DNA and HSA in the absence and presence of NiL_2 complex. The NiL_2-HSA and NiL_2-DNA complexes with the most negative free binding energy were considered as the initial conformations for the MD studies. GROMACS 5.1.2 package and Amber99 force field [30], [31] were used to carry out all MD studies. The partial atomic charges of NiL_2 were calculated using Gaussian 03 at the level of B3LYP/6-31G** [32], while other intramolecular force-field parameters were generated with ACPYPE [33] and VFFDT [34], respectively for the organic moiety and the metal center. Free biomacromolecules and NiL_2-biomacromolecule complexes were located in the cubic box with the periodic boundary conditions in the three directions. The solutes were placed in the center of box and the minimum distance between solute surface and the box was 1.0 nm. The box filled with TIP3P water molecules [35], [36], and the solvated systems were neutralized by adding appropriate amounts of sodium ions (Na^+) and chloride ions (Cl^-). After energy minimization using the steepest descent method, the systems were equilibrated for 200 ps at the temperature of 300 K. Finally, a 10 ns MD simulation was carried out at 1 bar and 300 K. Parrinello-Rahman barostate [37], [38] at 1 bar, Berendsen thermostat [39] at 300 K, 9 Å cut off for van der Walls and Coulomb interactions and the particle mesh Ewald (PME) method [40], [41] for long range electrostatics were used. The leap-frog algorithm with the 2 fs time step was used to integrate the equation of motions. Finally, an all-bond constrain was used to keep the NiL_2 from drifting and the atomic coordinates were recorded to the trajectory file every 0.5 ps for later analysis.

3.3. QM/MM study

Own N-layered Integrated Molecular Orbital and molecular Mechanics (ONIOM) methodology was employed to carry out QM/MM calculations. The ONIOM can be considered as a hybrid method, quantum mechanical method (QM) with a molecular mechanics (MM). This method is able to apply different ab initio or semi-empirical methods to different parts of a system and combine to produce reliable geometry and energy at reduced computational time [42]. In the two layers ONIOM method, the total energy (E_{ONIOM}) of the whole system is a sum of the three independent energy calculations: [43], [44]

$$E^{ONIOM2} = E^{high}_{model\ system} + E^{low}_{real\ system} - E^{low}_{model\ system} \quad (2)$$

Real system contains full geometry of the molecule and is considered as MM layer while the model system contains the chemically most important (core) part of the system that is considered as QM layer. Furthermore, the stability of respective adducts was obtained by the evaluation the interaction energy (ΔE), which is calculated by the following equation:

$$\Delta E = \Delta E_{Biomacromolecule/\ NiL_2} - \Delta E_{Biomacromolecule} - \Delta E_{NiL_2} \quad (3)$$

Where $\Delta E_{Biomacromolecule/NiL2}$, $\Delta E_{Biomacromolecule}$ and ΔE_{NiL2} are the energy of the optimized adduct of Biomacromolecule-NiL_2, Biomacromolecule and NiL_2, respectively. Biomacromolecule is DNA and HSA here as receptor. A two layers QM/MM method was used for all calculations. HSA and DNA are considered as low layer while the NiL_2 is considered as high layer in the current work. Molecular mechanics method (UFF) and semi empirical method (PM6) were selected for the low layer and the high layer, respectively.

4. Results

4.1. Analysis of synthesis and single crystal X-ray diffraction study

The reaction of Schiff base ligand with metal ion is shown in Scheme 1A. This complex was synthesized in water as solvent that is an important advantage for a drug candidate. The complex was obtained in good yield (more than 80%). The structure of complex was confirmed by Single-crystal X-ray diffraction and FT-IR techniques. The result of X-ray crystallography (ORTEP representation) is shown in Scheme 1B. The crystallographic data and selected bond lengths and angles are collected in Tables S1 and S2. In the solid state, NiL_2 is placed in a crystallographic center of symmetry that is right in the middle point of the Ni(II) in a planar-transoid conformation (Scheme 1B). The molecular unit is centrosymmetric and is made of equivalent halves. The crystallographic data reveal that the NiL_2 complex is four-coordinated by two phenolate oxygen and two imine nitrogen atoms of two Schiff base ligands. The Schiff base ligands are arranged with respect to each other in a trans orientation such that one allyl substituent lies above the

$[NiO_2N_2]$ plane and the other lies below. The C N bond distance is 1.296(3) Å [N(1)

C(7)], which are in consistent with a slight elongation of the C N double bond when are coordinated to a metal center [11], [12]. Examination of the Ni–ligand distances shows that the

Ni ⋯ N distance [Ni(1) N(1):1.9165(18)] is longer than the Ni ⋯ O distance [Ni(1)

O(1):1.8344(15) Å]. The bond angles [O(1) Ni(1) N(1) = 92.44(7)° and O(1) Ni(1)

N(1′) = 87.56(7)°] are close to 90°. The C C distance [C(9) C(10):1.264(4) Å] is well within the range is expected for double bonds are found in allyl derivatives [12].

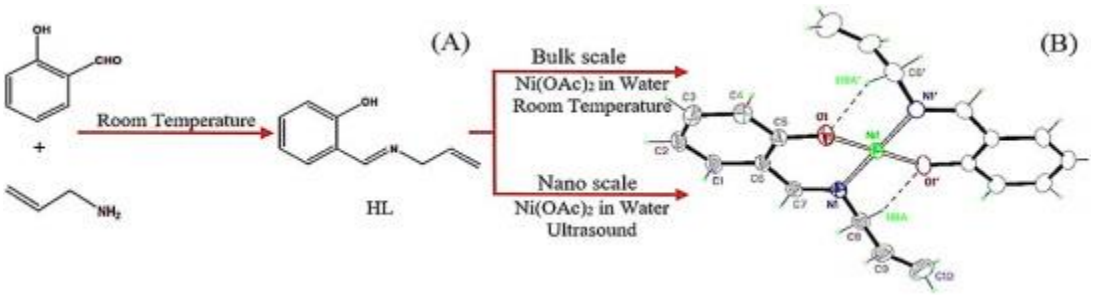

Scheme 1. (A) Synthetic routes for the preparation of NiL_2 in its bulk and nano-scale forms. (B) ORTEP representation of NiL_2. Displacement ellipsoids are drawn at the 50% probability level and H atoms are shown as small spheres with arbitrary radii. Hydrogen bonds are shown as dashed lines.

Although there are no classical hydrogen bonds in the structure, but two intramolecular C H ⋯ O contacts are observed in asymmetric unit of structure (Scheme 1B). These no classical hydrogen bonds and also distances and angles of these interactions are similar to those are seen in related complexes [11]. Also, FT-IR spectrum of NiL_2 complex is shown in Fig. S1.

4.2. Dynamic light scattering (DLS) and scanning electron microscopy (SEM) measurements

Fig. 1A shows the size distributions of NiL_2 dispersion. Three groups, one corresponding to very small particles (2–7 nm), one corresponding to small particles (100–300 nm) and the other representing large aggregates (5000–6000 nm), are observed in DLS distribution diagram. As it can be seen in this figure, about the 96% of synthesized particles have the size under 300 nm. Also, the morphology of synthesized nanoparticles was investigated under SEM. The particles exhibited an approximately plate shape (Fig. 1B).

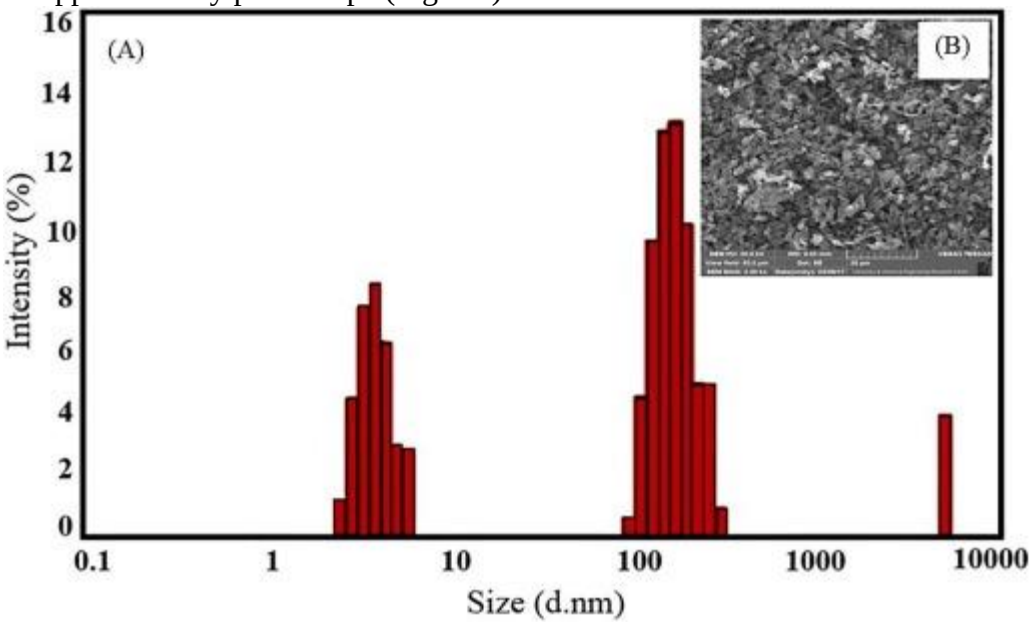

Fig. 1. (A) Hydrodynamic size distribution of nano-scale NiL_2 dispersion in water was measured by dynamic light scattering. (B) SEM image of the nano-scale NiL_2 complex.

4.3. MTT assay

The anticancer activity was considered as one of the most important potential applications of the compounds. To this aim, the cell viability percent of HeLa cancer cells after 48 h exposure to different concentrations of NiL_2 solution was first studied by MTT assay. The results (Fig. 2) are indicator of the dose dependent anticancer activity, as the cell mortality increased in the higher concentrations of the compound. In the best condition, more than 50% (53.59%) cell mortality was observed after 48 h exposure to 100 μM of the NiL_2 solution. Regarding to the obtained hopeful results for the NiL_2 solution and also, in order to increase the colloidal stability and suitability for the biomedical applications, the nano-scale NiL_2 was also synthesized and used for in vitro studies. The nano-scale compound could also represent the higher anticancer effects due to their probable increased bioavailability. About 20% differences for anticancer activity were observed between the NiL_2 solution and nano-scale compound dispersion. The maximum mortality of 79.36% HeLa cells obtained after 48 h exposure to 100 μM of nano-scale compound dispersion (Fig. 2). This result indicated that the anticancer activity of the compound is affected by its size. Regarding to the appropriate anticancer activity of the compound, further studies could be suggested for development of the potent anticancer agents.

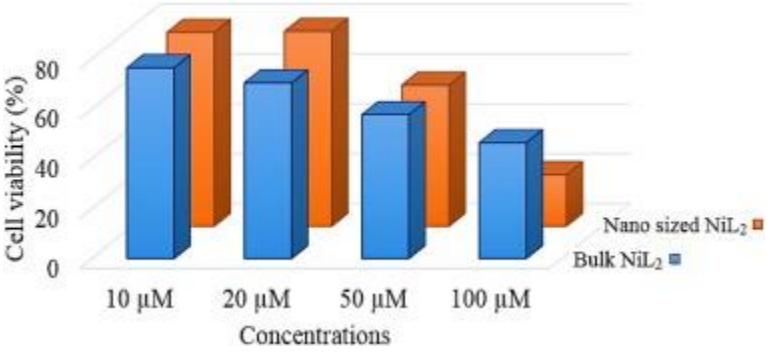

Fig. 2. The viability percentage of HeLa cancer cells after 48 h exposure to different concentrations (10, 20, 50 and 100 μM) of NiL_2 in both of scales.

4.4. Fluorescence study for interaction of nano-scale NiL_2 dispersion with CT-DNA and HSA

The fluorescence measurement as sensitive and effective technique for investigation the binding ability of nano-scale NiL_2 dispersion with CT-DNA and HSA was performed. Fig. 3A represents the fluorescence quenching of DNA-Ethidium Bromide (EB) spectrum by adding nano-scale NiL_2 dispersion. Hydrogen transfer from one of the amino groups of EB into the solution causes non-radiative decay and a weak fluorescence emission. Although, a significant increase in fluorescence intensity of EB is observed in the presence of DNA due to intercalation of the EB molecules into the double helix of DNA [45], [46]. NiL_2 can displace EB in a non-competitive manner by changing the DNA conformation. The DNA-bound EB molecules are converted to their free form in solution and causes fluorescence quenching.

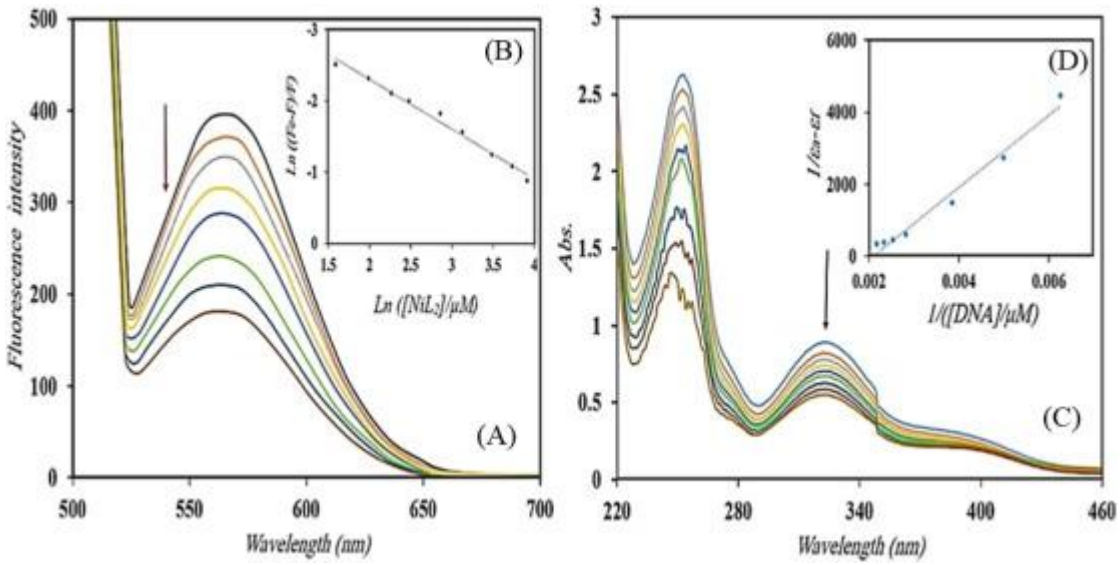

Fig. 3. (A) Changes in the fluorescence spectra of DNA-EB in the presence of increasing amounts of NiL_2 in Tris buffer pH = 7.5 ([DNA] = 25 μM, [NiL_2] = 250 μM). (B) Plot of Ln(($F_0 - F$)F) versus Ln[NiL_2]. (C) Absorption spectra of nano-scale NiL_2 complex in the presence of various amounts of DNA ([NiL_2] = 200 μM, [DNA] = 1 mM). (D) Plot of $1 / \varepsilon_a - \varepsilon_f$ versus (1 / [DNA])).

On the other hand, the intrinsic fluorescence of HSA is mainly due to the tryptophan residue [47]. The fluorescence intensity of protein was quenched through the addition of the nano-scale NiL_2 dispersion. This implies that the compound strongly interacts with HSA, leading to changes of microenvironment around the Trp-214 residue in HSA [48], [49]. Fig. 4A represents the fluorescence quenching of HSA at the presence of various amount of the compound. The Scachard equation was used to obtain the binding affinity of nano-scale NiL_2 dispersion to DNA and HSA: [50]

$$\mathrm{Ln}\left(\frac{F_0-F}{F}\right) = \mathrm{Ln}(K_\mathrm{b}) + n\,\mathrm{Ln}\,[\mathrm{Q}] \qquad (4)$$

where, F_0 and F are the fluorescence intensity of biomacromolecule in the absence and presence of the compound, respectively. [Q] Is the concentration of quencher that quencher is nano-scale NiL_2 dispersion here. "K_b" is binding constant and is obtained from the plot of Ln(($F_0 - F$)/F) versus Ln [Q] as y-intercept. These plots are shown in Figs. 3B and 4B for DNA and HSA respectively. "n" is the number of binding site per biomacromolecule and is determined as slope of the plot. The values of n are nearly 1 for NiL_2 with both of biomacromolecules, indicating that the compound binds to DNA and HSA with molar ratio of 1:1. The calculated results are shown in Table 1.

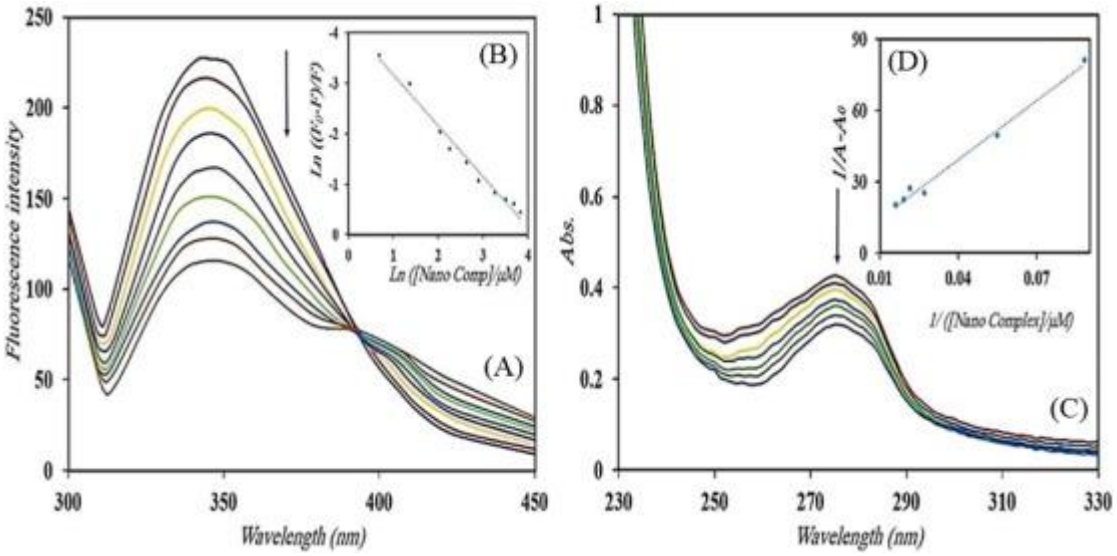

Fig. 4. (A) Changes in the fluorescence spectra of HSA in the presence of increasing amounts of nano-scale NiL_2 in phosphate buffer pH = 7 ([HSA] = 10 μM, [NiL_2] = 200 μM). (B) Plot of Ln(($F_0 - F$) / F) versus Ln[NiL_2]. (C) Absorption spectra of HSA in the presence of various amounts of nano-scale NiL_2 ([HSA] = 10 μM, [NiL_2] = 200 μM). (D) Plot of $1 / A - A_0$ versus 1 / [NiL_2].

Table 1. The DNA and HSA-binding constants (K_b), the number of binding sites (n), the Stern-Volmer constants (K_{sv}) and the quenching rate constants (k_q) of the NiL_2.

Type of biomolecule	$K_b(M^{-1})$ (fluorescence)	$K_b(M^{-1})$ (UV–Vis)	n	$K_{SV}(M^{-1})$	$k_q(M^{-1}\cdot S^{-1})$
CT-DNA	2.45×10^4	2.24×10^3	0.7	0.76×10^4	0.76×10^{12}
HSA	1.55×10^4	7.32×10^3	1.01	1.37×10^4	1.37×10^{12}

To determine the interaction mode of the nano-scale NiL_2 dispersion with CT-DNA and HSA, the Stern–Volmer quenching plot was obtained by monitoring the fluorescence quenching of biomacromolecules with increasing the concentration of the compound according to the Stern–Volmer equation: [51]

$$\frac{F_0}{F} = 1 + K_{sv}[Q] = 1 + k_q \tau [Q] \quad (5)$$

where, F_0 and F are the fluorescence intensity of biomacromolecules in the absence and presence of the compound, respectively. K_{sv} is the Stern-Volmer quenching constant, k_q is the quenching rate constant of biomacromolecules and τ is the average lifetime of biomacromolecules without quencher which is typically equal to 10^{-8} s for biomacromolecules. K_{sv} is determined from the plot of F_0/F vs. [Q] (Figs. S2 and S3). Also, the values of K_{sv} were obtained for both of biomacromolecules and are presented in Table 1.

Fluorescence quenching is classified as two mechanisms: static quenching and dynamic quenching. In the static mechanism, the fluorophore and the quencher collide together in the ground state while fluorophore and quencher collide together in the excited state in dynamic

mechanism. Linearity of the Stern-Volmer plots indicates that fluorescence quenching has only one mechanism: dynamic or static [50]. In this study, the values of k_q were obtained about 10^{12} $M^{-1} \cdot S^{-1}$ for DNA and HSA. These values are greater than limiting diffusion rate constant of the diffusional quenching for biopolymers (2×10^{10} $M^{-1} \cdot S^{-1}$) and support that quenching fluorescence of DNA and HSA occurs by static mechanism.

4.5. Thermodynamic parameters and determination of nature of interaction forces

According to the Ross and Subramanian report, there are four non-covalent effective forces in interaction between compounds and biomacromolecules including hydrophobic, hydrogen, electrostatic and Vander-waals interactions [52]. For determination the type of interactions NiL_2 with biomacromolecules, the thermodynamic parameters were calculated using the following equations:

$$\mathrm{Ln}\, K = -\frac{\Delta H^\circ}{RT} + \frac{\Delta S^\circ}{R} \quad (6)$$

$$\Delta G^\circ = \Delta H^\circ - T\,\Delta\, S^\circ = -RT\mathrm{Ln}\, K \quad (7)$$

where, R is the gas public constant, T is the experimental temperature, K is binding constant at the corresponding temperature, $\Delta G°$, $\Delta H°$ and $\Delta S°$ are the free energy changes, the enthalpy changes and the entropy changes, respectively.

$\Delta H°$ and $\Delta S°$ were estimated from the plot LnK vs. $1/T$ as slop and y-intercept, respectively. Also, $\Delta G°$ was obtained using Eq. (7). The estimated Values are summarized in Table 2. The positive $\Delta H°$ and $\Delta S°$ values for both of biomacromolecules indicated that hydrophobic interactions have the main role in binding of nano-scale NiL_2 dispersion to CT-DNA and HSA. Also, the negative $\Delta G°$ values in all experimental temperatures illustrated that the interactions occurred spontaneously. Plots of LnK vs. $1/T$ for both of biomacromolecules are present in Figs. S4 and S5.

Table 2. The thermodynamic parameters for binding of NiL_2 to HSA and CT-DNA, including binding constants at the corresponding temperatures (K_b), free energy change ($\Delta G°$), enthalpy change ($\Delta H°$) and entropy change ($\Delta S°$).

Type of biomolecule	Temperature (°C)	K_b	$\Delta G°$ (kJ/mol)	$\Delta H°$ (kJ/mol)	$\Delta S°$ (J/mol·K)
	25	2.45×10^4	− 25.05	76.11	339.32
CT-DNA	35	8.37×10^4	− 29.03	76.11	341.25
	45	1.67×10^5	− 31.82	76.11	339.28
	25	1.55×10^4	− 23.92	61.83	287.60
HSA	35	5.57×10^4	− 27.99	61.83	291.51
	45	7.36×10^4	− 29.64	61.83	287.52

4.6. UV–Vis absorption

Absorption titration experiment as an operational and very easy method was also carried out for more investigation of HSA and DNA binding of NiL_2. Generally, hyperchromic or hypochromic effect and red or blue shift are observed in the UV–Vis spectrum of a drug upon its DNA-binding. Hypochromic and red shift are indicative of intercalation mode involving an interaction between π*-orbital of drug with π-orbital of DNA base pairs [53]. Therefore, energy level of π*-orbital of drug decreases which causes red shift in its UV–Vis spectrum. Furthermore, the coupled π*-orbital is filled and so the probability of electron transition is decreased and hypochromic is observed [53], [54]. While a groove binding or electrostatic interaction leads to hyperchromic effect along with blue shift [55].

The absorption titration was carried out by adding various amount of CT-DNA to nano-scale NiL_2 dispersion. The absorption spectrum of nano-scale NiL_2 dispersion indicates two absorption bands at 250 and 320 nm that attributed to $\pi \rightarrow \pi^*$ and $n \rightarrow \pi^*$ transitions, respectively (Fig. 3C). The band in 320 nm was chosen to investigate the interaction of nano-scale NiL_2 dispersion with DNA. Although, the existence of hypochromic effect in UV–Vis spectrum attributed to intercalation mode, some of reports predicate that hyperchromic effect is relevant to groove binding due to the changes in solvent distribution and the orientation effect in moving into the more hydrophobic environment of groove [55]. In order to assess the binding ability of the compound to CT-DNA, the binding constant (K_b) was estimated by monitoring the changes of absorbance with increasing concentration of CT-DNA and using the following equation: [56]

$$\frac{1}{(\varepsilon_a-\varepsilon_f)} = \frac{1}{(\varepsilon_b-\varepsilon_f)} + \frac{1}{K_b(\varepsilon_b-\varepsilon_f)} \times \frac{1}{[\mathrm{DNA}]} \quad (8)$$

where, ε_f and ε_a are the molar absorbance coefficient of NiL_2 in the absence and presence of CT-DNA, respectively. ε_b is the obtained molar absorbance coefficient in saturation and [DNA] is the concentration of CT-DNA. The plot of $1/(\varepsilon_a - \varepsilon_f)$ versus 1/[DNA] gives K_b as ratio of y-intercept to slop (Fig. 3D and Table 1).

Also, the absorption titration was carried out to investigate the interaction of HSA and nano-scale NiL_2 dispersion. Fig. 4C shows UV–Vis spectra of HSA in the absence and presence of nano-scale NiL_2 dispersion. There is one peak at 278 nm is assigned to $\pi \rightarrow \pi^*$ transition of the phenyl rings in aromatic amino acids (Trp, Tyr and Phe) [55]. By addition of the nano-scale NiL_2 dispersion, a hypochromic effect is observed in HSA spectrum. This result shows that the aromatic amino acids of HSA were exposed to an aqueous environment upon binding to the compound. Following equation was used to investigate the binding affinity of NiL_2 to HSA at 278 nm: [57]

$$\frac{1}{A-A_0} = \frac{1}{A_{\max}-A} + \frac{1}{K_b(A_{\max}-A)} \times \frac{1}{[M]} \quad (9)$$

where, A_0 and A are the absorbance of HSA in the absence and presence of the compound, respectively. A_{max} is the obtained absorbance at saturation and [M] is the concentration of nano-scale NiL_2 dispersion. The plot of $1 / (A - A_0)$ versus $1 / [M]$ gives K_b as ratio of y-intercept to slope (Fig. 4D and Table 1).

Generally, binding constant of a drug with a carrier protein such as HSA should be high enough to bind and transfer through body. Moreover, in order to release a drug since arrival at its target, binding constant should not be too high [58]. With respect to above, HSA binding constant of the NiL_2 is in a good range ($2–10 \times 10^4$) and also is comparable to analogue compounds and some potent drugs [12].

In addition, our compound is uncharged which is an advantage for a drug. The researches show that the unionized drugs are soluble in lipid and are capable to cross through the membrane's lipid bilayer while the ionized analogue species fail to cross [51].

4.7. Circular dichroism (CD) spectroscopy

The CD spectra of HSA and DNA in free and bonded to nano-scale NiL_2 complex states are shown in Fig. 5. The CD spectrum of HSA indicates two negative peaks at 208 and 222 nm which are characteristic absorption peaks of α-helical structure of protein attributed to the n-π* transfer for the bonds of the

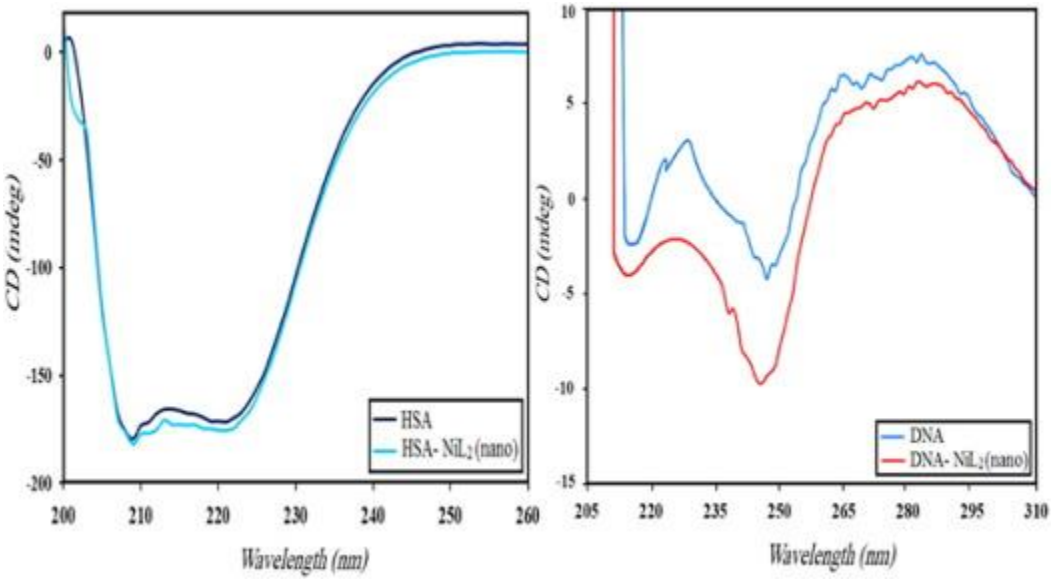

Fig. 5. The CD spectra of HSA and DNA in the absence and presence of nano-scale NiL_2 complex in the molar ratio [complex] / [biomolecule] = 1.

α-helix [59]. According to Fig. 5, the intensity of HSA peak has been altered slightly due to binding nano-complex. Thus, there is no considerable structural change for HSA due to its interaction with NiL_2. The CD spectrum of free double stranded DNA exhibits four marker peaks at about 210 (negative), 222 (positive), 245 (negative) and 280 nm (positive). The positive peak at about 280 nm due to base stacking and negative peak at 245 nm due to polynucleotide helicity are main peaks of DNA for its B-type, which are highly sensitive towards the DNA interaction with small molecules [60]. Fig. 5 shows that the intensity of DNA peaks has been altered due to binding nano-complex more than the changes in HSA CD spectrum. This observation confirms that the interaction of NiL_2 with DNA is stronger than its interaction with HSA that is in consistent with the fluorescence results.

4.8. Viscosity measurement

To further verify the interaction mode of the nano-scale NiL_2 dispersion with CT-DNA, viscosity measurements of DNA upon addition of the nano-scale NiL_2 dispersion were carried out. A classical intercalative mode causes an increase in the DNA viscosity due to increasing of overall length of DNA [11]. On the other hand, groove binding and electrostatic interactions could bend

the DNA helix, reduce its length and cause the reduction or no change in the DNA viscosity [11]. The effect of the nano-scale NiL_2 dispersion complex on the viscosity of CT-DNA is demonstrated in Fig. S6. As it can be seen, the viscosity of DNA decreased until molar ratio of $[NiL_2]$ / [DNA] = 0.25 and remained constant with increasing amounts of the complex, indicating the binding mode of NiL_2 may be groove binding. This result is in good agreement with molecular docking and spectroscopic results.

4.9. Molecular docking studies

Molecular docking is a valuable technique to predict the stable structure of receptor-ligand complex for better recognition of the interaction details in drug discovery process. This method is frequently employed as virtual searching tools in primary steps of drug design and development. In order to find out the preferred location of the compound on DNA and HSA, molecular docking studies were carried out. Table 3 represents the obtained binding modes and docking energies of the compound during its interaction with both of the biomacromolecules. The docked model suggests that NiL_2 binds with the minor groove of DNA with standard binding free energy ($\Delta G°$) of -7.69 kcal·mol^{-1}. This score is related to the docking cluster with maximum population and minimum binding energy. Also, intermolecular energy which covers H-bonding interactions, van der waals, desolvation and electrostatic energies, was estimated as -8.79 kcal·mol^{-1} [61]. Also, docking studies showed that there is one H-bond between O atom of the NiL_2 and DG4 nucleotide.

Table 3. Molecular docking results for the interaction of NiL_2 complex with DNA and HSA.

Type of biomolecule	binding energy (kcal·mol^{-1})	View of binding site	Zoom in binding site
DNA	-7.69		
HSA	-5.59		

The results of molecular docking for interaction of NiL_2 and HSA indicate that the compound is situated in the warfarin binding site, in IIA subdomain (Table 3). The NiL_2 complex is bound to the HSA with the binding energy of -5.59 kcal·mol^{-1}. Also, the intermolecular energy for HSA is -6.69 kcal·mol^{-1}. The amino acids residues with major role in the stability of NiL_2-HSA system are LYS199, TRP214, ARG218, ARG222, LEU219, ALA291, ILE290, PHE223, ILE264, LEU260, ARG257, GLU153, TYR150 and ALA261. According to the obtained results, there is one hydrogen bond between N atom of the NiL_2 complex with ARG222 residue of HSA. Moreover, four π-cation interactions were formed between phenyl rings of the compound with residues of the binding site. The participant residues of HSA in π-cation interactions are ARG222, LYS199 and ARG257.

4.10. Molecular dynamics simulation

The beginning structures for the MD analyses were selected from the conformations with lowest docking energies. The stability of the system (biomacromolecule and compound) properties was examined by means of RMS deviations (RMSD) of unbound and ligand conjugated biomacromolecule with respect to the initial structure, RMS fluctuations (RMSF), the solvent accessible surface area (SASA) of biomacromolecule, radius of gyration (R_g) and number of H-bonds. Preliminary simulations over 10 ns time were performed on DNA and HSA with

NiL_2. Table 4 provides the average values of RMSD, SASA, R_g and number of H-bonds of the HSA and HSA-NiL_2 systems. Fig. 6 presents time dependence of RMSD, R_g, RMSF and H-bond values of HSA and HSA-NiL_2 systems. Fig. 6A indicates that the trajectories of both systems are stable and their RMSD reached equilibrium and fluctuated around its mean value after about 5 ns simulation time. Figs. 6B and S7 show that complexation with NiL_2 changed the structure of HSA when compared to free protein. It can be clearly seen that the R_g and SASA were larger upon binding of the NiL_2 suggesting a less compact structure of HSA in the presence of NiL_2. Decreasing the number of intramolecular H-bonds is another evidence that confirms a less compact structure of HSA in the presence of NiL_2 (Fig. 6C).

Table 4. The average values of RMS deviations (RMSD), the solvent accessible surface area (SASA), the radius of gyration (R_g) and number of H-bonds of the HSA and HSA-NiL_2 systems.

System	RMSD (nm)	SAS (nm^2)	R_g (nm)	Number of H-bond
HSA	0.25 ± 0.05	298.22 ± 3.70	2.69 ± 0.02	481.50 ± 10.97
HSA-NiL_2	0.28 ± 0.04	303.69 ± 3.79	2.71 ± 0.01	462.80 ± 11.20

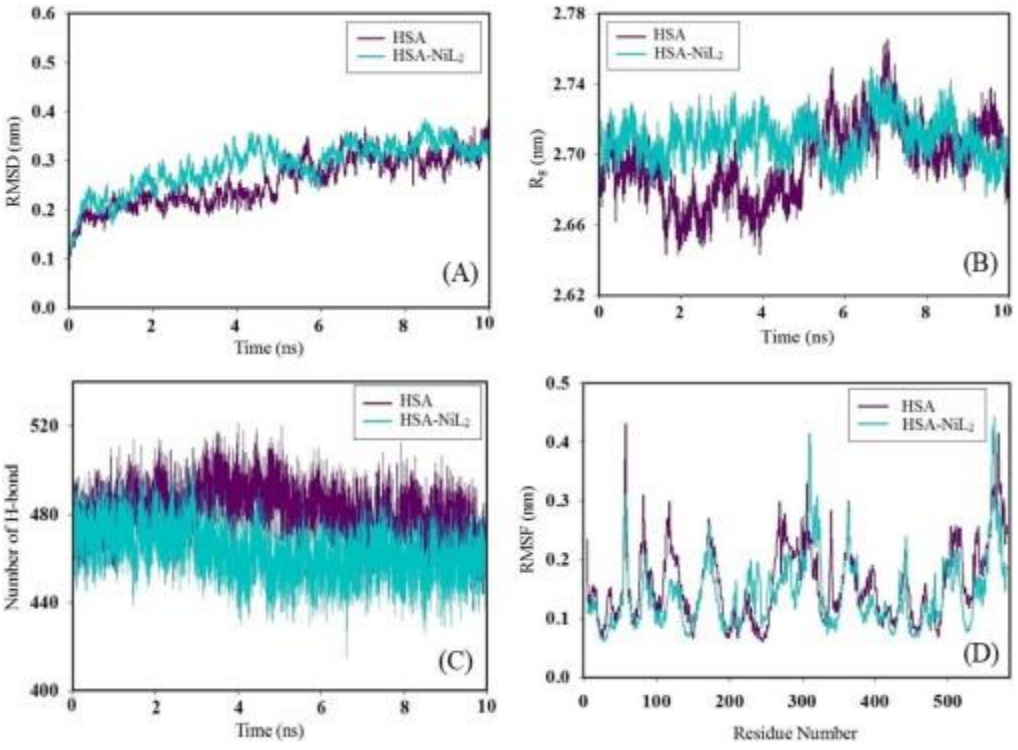

Fig. 6. (A) Time dependence of RMSD. RMSD values for HSA and HSA-NiL_2 complex during 10 ns MD simulation. (B) Time-evolution of radius of gyration (Rg) for HSA and HSA-NiL_2 complex during 10 ns MD simulation. (C) The number of Intramolecular H-bonds for HSA and HSA-NiL_2 complex during 10 ns MD simulation. (D) RMSF values of HSA and HSA-NiL_2 complex plotted against residue numbers.

Also, local protein mobility was analyzed by calculating the time averaged RMSF values of free HSA and HSA-NiL_2 complex and was plotted against residue numbers based on the last 5000 ps trajectory (Fig. 6D). The profiles of atomic fluctuations were found to be very similar to those of free HSA and HSA-NiL_2 complex. RMSF highlights the conformational adjustments of the protein structure, in conjunction with NiL_2 conformational adaptation to its binding sites. The results indicate that the residues that were in contact with the NiL_2 are stable and have low RMSF values suggesting that the structure of drug binding site remains rigid during simulation. Hence, it can be concluded that the interactions of protein and NiL_2 were stable during the simulation time.
Fig. 7 presents time dependence of RMSD and RMSF values of DNA and DNA-NiL_2 systems. Fig. 7A indicates that the trajectories of both systems are stable and their RMSD reached equilibrium and fluctuated around its mean value after about 1 ns simulation time. Also, local DNA mobility was analyzed by calculating the time averaged RMSF values of free DNA and DNA-NiL_2 complex and was plotted against atom numbers based on the last 8000 ps trajectory (Fig. 7B). The results indicate that the atoms of DNA bound NiL_2 are stable and have lower RMSF values than the free DNA. Hence, it can be concluded that the interactions of DNA and NiL_2 were stable during the simulation time.

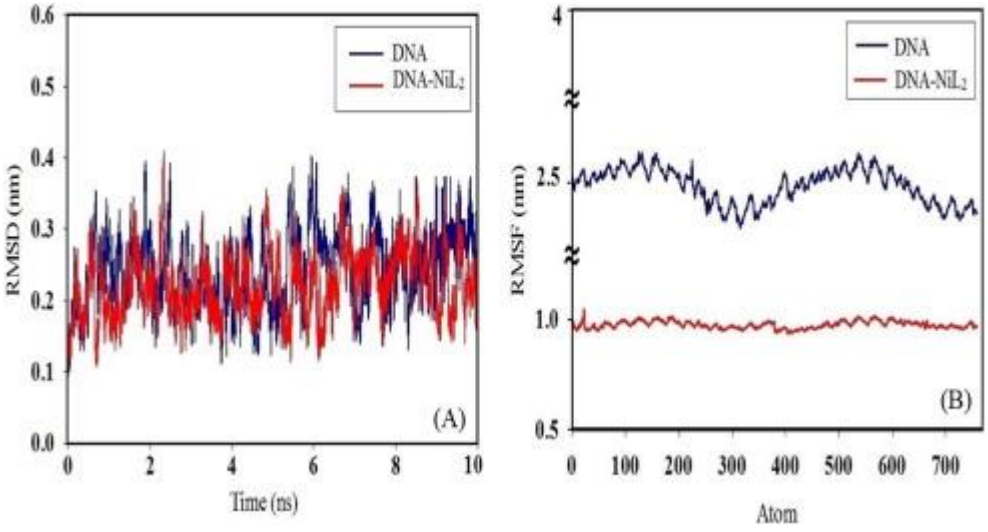

Fig. 7. (A) Time dependence of RMSD. RMSD values for DNA and DNA-NiL_2 complex during 10 ns MD simulation. (B) RMSF values of DNA and DNA-NiL_2 complex plotted against atom numbers.

4.11. QM/MM studies

In this work, a two-layer ONIOM calculations including (PM6: UFF) were employed to perform QM/MM studies. The molecular mechanics (MM) was described using the UFF force field for HSA and DNA (low layer) while semi-empirical quantum mechanics (QM) method (PM6) was chosen for the NiL_2 (high layer). The most stable geometries obtained from the molecular docking calculations were opted as starting points of HSA- and DNA- NiL_2 for the two-layer ONIOM studies. All calculations were performed using Gaussian 03 quantum chemistry package. The partial atomic charges on the atoms of the NiL_2, DNA and HSA were considered to reoptimize the

optimized geometries. The van der Waals (vdw) and electrostatic interaction were considered in structure optimization. Moreover, the polarization of the wave function of the NiL_2 was considered to obtain more truthful geometries [12]. The results of ONIOM calculations represented that structure of the NiL_2 deviates from its initial geometry due to the binding to DNA and HSA. Along with the interaction of NiL_2 with biomacromolecules some bond lengths and bond angles are changed. Such the changes can be indicative of the strength of the interaction between biomacromolecules and NiL_2. Fig. 8, Fig. 9 show the changes take place in some geometrical parameters including bond angles of NiL_2 along with binding to DNA and HSA. The calculated binding energies (ΔE) of NiL_2 and biomacromolecules are present in Table 5 for DNA and HSA. In view of considering the polarization of the NiL_2 in electrostatic field of HSA and DNA in QM/MM calculation, this energy is more accurate than calculated energy by molecular docking method.

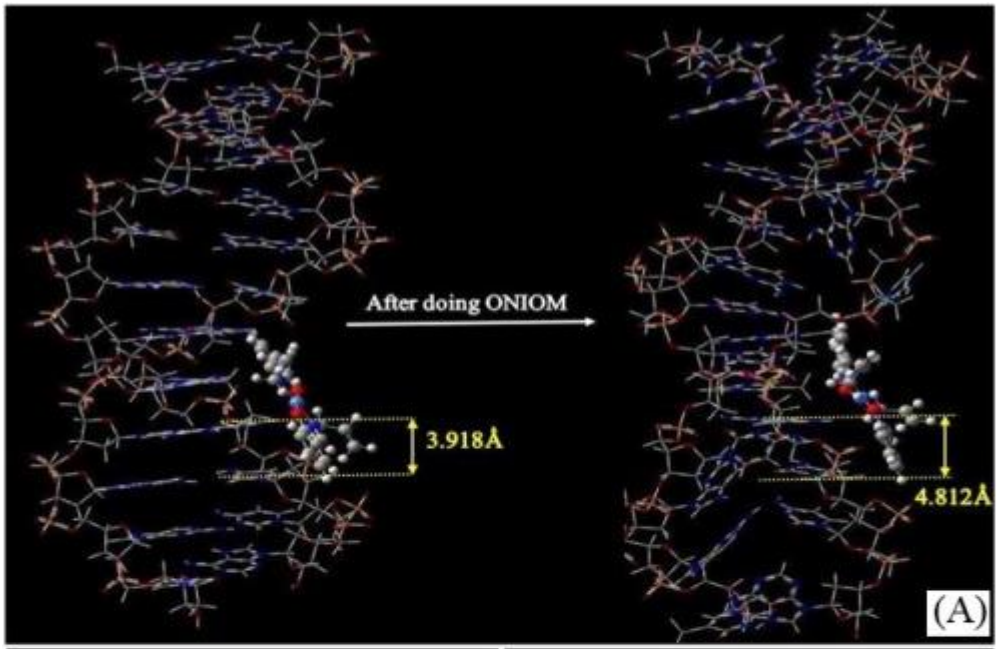

Type of Angle	Angle (before ONIOM)/Degree	Angle (after ONIOM)/Degree
α	88.17	84.52
β	116.37	123.24
γ	125.02	115.84

Fig. 8. (A) The structure of the NiL_2 complex and DNA optimized considering charged embedding of MM part in QM part in the gas phase. (B) The changes of structural parameters of NiL_2 during binding to DNA.

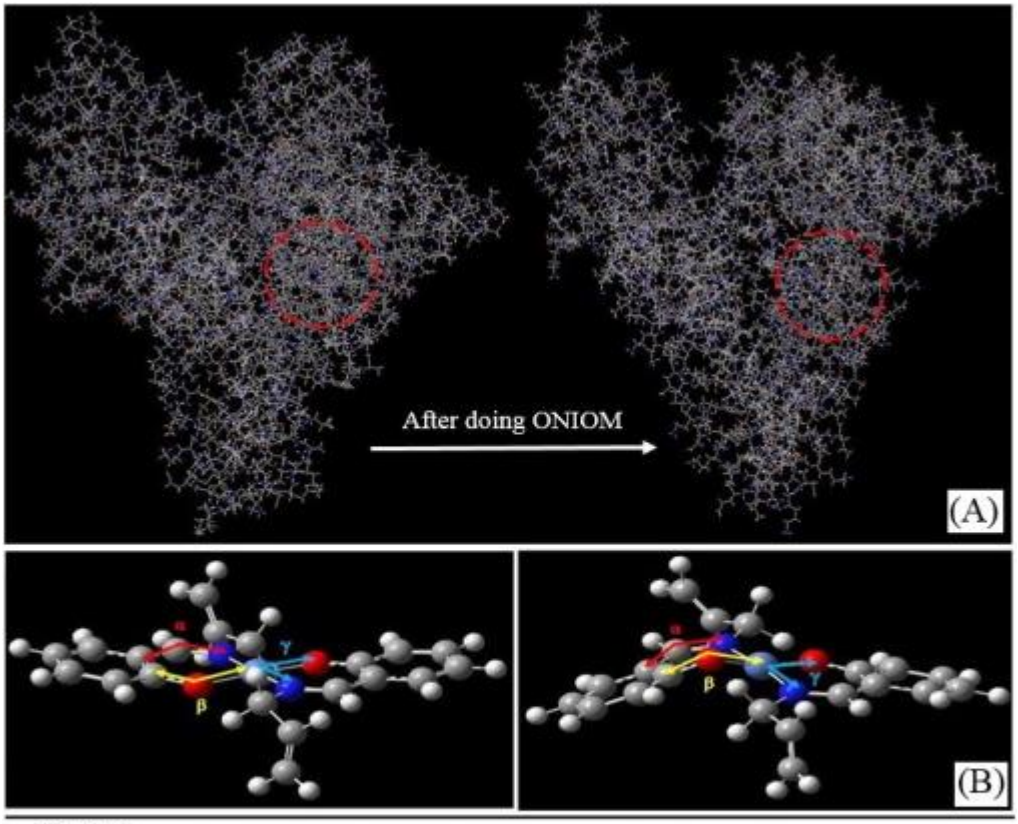

Type of Angle	Angle (before ONIOM)/Degree	Angle (after ONIOM)/Degree
α	127.65	123.30
β	130.11	114.60
γ	93.92	97.93

Fig. 9. (A) The structure of NiL_2 complex and HSA optimized considering charged embedding of MM part in QM part in the gas phase. (B) The changes of structural parameters of NiL_2 during binding to HSA.

Table 5. The calculated binding energies (ΔE) of NiL_2 with HSA and DNA.

System	NiL_2(PM6) (kcal·mol^{-1})	Biomolecule(UFF) (kcal·mol^{-1})	ΔE (kcal·mol^{-1})
NiL_2-HSA	− 2.4473	− 4913.25	4957.091
NiL_2-DNA	− 2.4473	2823.01	− 2744.14

5. Conclusions

In conclusion, we have synthesized a new nano-scale Schiff base Ni(II) complex in water as a green solvent and at ambient temperature. The structure of complex has been established by using single crystal X-ray diffraction analysis. The crystallographic data reveal that NiL_2 is placed in a crystallographic center of symmetry that is right in the middle point of the Ni(II) in a planar-transoid conformation. The MMT assay results indicated that the anticancer activity of the compound is affected by its size. The DNA- and HSA-binding of the NiL_2 was also investigated, using both experimental (fluorescence quenching, CD analysis, viscosity measurements and UV–Vis spectroscopy) and computational methods (molecular docking, molecular dynamics simulation and ONIOM). The obtained HSA- and DNA-binding constant values from experimental and computational methods stated that the binding of Ni(II) complex to the minor groove of DNA and warfarin binding site of protein by formation of hydrogen bond, π-cation and hydrophobic interactions. MD simulation studies revealed that complexation with NiL_2 changed the structure of HSA when compared to free protein. Finally, the ONIOM results showed that the structural parameters of the compound changed along with binding to DNA and HSA, indicating the strong interaction between the compound and these biomacromolecules.

Acknowledgment

The financial supports of the research council of University of Isfahan are gratefully acknowledged.

Appendix A. Supplementary data

CCDC 1547057 contains the supplementary crystallographic data for NiL2. Copies of the data can be obtained, free of charge, on application to CCDC, 12 Union Road, Cambridge CB21EZ, UK (Fax: +44 1223 336033 or e-mail: deposit@ccdc.cam.ac.uk).

References

[1] S.P. Gautam, A. Verma, PAMAM dendrimers: novel polymeric nanoarchitectures for solubility enhancement of candesartan cilexetil, J. Pharm. Sci. 1 (2012) 1–4.

[2] E.C. Dreaden, A.M. Alkilany, X. Huang, C.J. Murphy, M.A. El-Sayed, The golden age: gold nanoparticles for biomedicine, Chem. Soc. Rev. 41 (2012) 2740–2779.

[3] S. Jain, D. Hirst, J. O'sullivan, Gold nanoparticles as novel agents for cancer therapy, Br. J. Radiol. 85 (2014) 101–113.

[4] S. Parveen, R. Misra, S.K. Sahoo, Nanoparticles: a boon to drug delivery, therapeutics, diagnostics and imaging, Nanomed. Nanotech. Biol. Med. 8 (2012) 147–166.

[5] J. Panyam, V. Labhasetwar, Biodegradable nanoparticles for drug and gene delivery to cells and tissue, Adv. Drug Deliv. Rev. 55 (2003) 329–347.

[6] H. Keypour, A. Shooshtari, M. Rezaeivala, F.O. Kup, H.A. Rudbari, Synthesis of two new N2O4 macroacyclic Schiff base ligands and their mononuclear complexes: spectral, X-ray crystal structural, antibacterial and DNA cleavage activity, Polyhedron 97 (2015) 75–82.

[7] M. Abo-Aly, A. Salem, M. Sayed, A.A. Aziz, Spectroscopic and structural studies of the Schiff base 3-methoxy-N-salicylidene-o-amino phenol complexes with some transition

metal ions and their antibacterial, antifungal activities, Spectrochim. Acta A 136 (2015) 993–1000.
[8] N. El-wakiel, M. El-keiy, M. Gaber, Synthesis, spectral, antitumor, antioxidant and antimicrobial studies on Cu (II), Ni (II) and Co (II) complexes of 4-[(1Hbenzoimidazol-2-ylimino)-methyl]-benzene-1, 3-diol, Spectrochim. Acta A 147 (2015) 117–123.
[9] W.H. Mahmoud, R.G. Deghadi, G.G. Mohamed, Novel Schiff base ligand and itsmetal complexes with some transition elements. Synthesis, spectroscopic, thermal analysis, antimicrobial and in vitro anticancer activity, Appl. Organomet. Chem. 30 (2016) 221–230.
[10] L.H.A. Rahman, A.M. Abu-Dief, S.K. Hamdan, A.A. Seleem, Nano structure iron (II) and copper (II) Schiff base complexes of a NNO-tridentate ligand as new antibiotic agents: spectral, thermal behaviors and DNA binding ability, Int. J. Nano. Chem. 1 (2015) 65–77.
[11] Z. Kazemi, H.A. Rudbari,M. Sahihi, V. Mirkhani, M. Moghadam, S. Tangestaninejad, I. Mohammadpoor-Baltork, G. Azimi, S. Gharaghani, A.A. Kajani, Synthesis, characterization and separation of chiral and achiral diastereomers of Schiff base Pd (II) complex: a comparative study of their DNA-and HSA-binding, J. Photochem. Photobiol. B 163 (2016) 246–260.
[12] Z. Kazemi, H.A. Rudbari,M. Sahihi, V. Mirkhani, M. Moghadam, S. Tangestaninejad, I. Mohammadpoor-Baltork, S. Gharaghani, Synthesis, characterization and biological application of four novel metal-Schiff base complexes derived from allylamine and their interactions with human serum albumin: experimental, molecular docking and ONIOM computational study, J. Photochem. Photobiol. B 162 (2016) 448–462.
[13] I. Khosravi, F. Hosseini, M. Khorshidifard, M. Sahihi, H.A. Rudbari, Synthesis, characterization, crystal structure and HSA binding of two new N, O, O-donor Schiff-base ligands derived from dihydroxybenzaldehyde and tert-butylamine, J. Mol. Struct. 1119 (2016) 373–384.
[14] J. Anacona, J.L. Rodriguez, J. Camus, Synthesis, characterization and antibacterial activity of a Schiff base derived from cephalexin and sulphathiazole and its transition metal complexes, Spectrochim. Acta A 129 (2014) 96–102.
[15] Y. Mohini, R. Prasad, M. Karuna, Y. Poornachandra, C.G. Kumar, Synthesis, antimicrobial and anti-biofilm activities of novel Schiff base analogues derived from methyl-12-aminooctadec-9-enoate, Bioorg. Med. Chem. Lett. 24 (2014) 5224–5227.
[16] T. Eitinger, M.-A. Mandrand-Berthelot, Nickel transport systems in microorganisms, Arch. Microbiol. 173 (2000) 1–9.
[17] S.W. Ragsdale, Nickel biochemistry, Curr. Opin. Chem. Biol. 2 (1998) 208–215.
[18] E. Zangrando, M. Islam, M.A.-A.A. Islam, M. Sheikh, M. Tarafder, R. Miyatake, R. Zahan, M. Hossain, Synthesis, characterization and bio-activity of nickel (II) and copper (II) complexes of a bidentate NS Schiff base of S-benzyl dithiocarbazate, Inorg. Chim. Acta 427 (2015) 278–284.
[19] C. Stoe, X-AREA, Version 1.30, Programfor the Acquisition and Analysis of Data, Stoe & Cie GmbH, Darmatadt, Germany, 2005.
[20] C. Stoe, X–RED: Programfor Data Reduction and Absorption Correction, Version 1.28 b, Stoe & Cie GmbH, Darmatadt, Germany, 2005.

[21] C. Stoe, X-SHAPE, Version 2.05, Program for Crystal Optimization for Numerical Absorption
Correction, Stoe & Cie GmbH, Darmatadt, Germany, 2004.
[22] M.C. Burla, R. Caliandro, M. Camalli, B. Carrozzini, G.L. Cascarano, L. De Caro, C. Giacovazzo, G. Polidori, R. Spagna, SIR2004: an improved tool for crystal structure determination and refinement, J. Appl. Crystallogr. 38 (2005) 381–388.
[23] G.M. Sheldrick, Crystal structure refinement with SHELXL, Acta Crystallogr. C: Struct. Chem. 71 (2015) 3–8.
[24] A.A. Kajani, A.-K. Bordbar, S.H.Z. Esfahani, A. Razmjou, Gold nanoparticles as potent anticancer agent: green synthesis, characterization, and in vitro study, RSC Adv. 6 (2016) 63973–63983.
[25] M. Reichmann, S. Rice, C. Thomas, P. Doty, A further examination of the molecular weight and size of desoxypentose nucleic acid, J. Am. Chem. Soc. 76 (1954) 3047–3053.
[26] K. Zheng, F. Liu, X.-M. Xu, Y.-T. Li, Z.-Y.Wu, C.-W. Yan, Synthesis, structure and molecular
docking studies of dicopper (II) complexes bridged by N-phenolato-N′-[2-(dimethylamino) ethyl] oxamide: the influence of terminal ligands on cytotoxicity and reactivity towards DNA and protein BSA, New J. Chem. 38 (2014) 2964–2978.
[27] C.N. Pace, F. Vajdos, L. Fee, G. Grimsley, T. Gray, How to measure and predict the molar absorption coefficient of a protein, Protein Sci. 4 (1995) 2411–2423.
[28] S. Bi, Y. Sun, C. Qiao, H. Zhang, C. Liu, Binding of several anti-tumor drugs to bovine serum albumin: fluorescence study, J. Lumin. 129 (2009) 541–547.
[29] G.M. Morris, D.S. Goodsell, R.S. Halliday, R. Huey, W.E. Hart, R.K. Belew, A.J. Olson, Automated docking using a Lamarckian genetic algorithm and an empirical binding free energy function, J. Comput. Chem. 19 (1998) 1639–1662.
[30] A. Pérez, I. Marchán, D. Svozil, J. Sponer, T.E. Cheatham, C.A. Laughton, M. Orozco, Refinement of the AMBER force field for nucleic acids: improving the description of α/γ conformers, Biophys. J. 92 (2007) 3817–3829.
[31] J.Wang, R.M.Wolf, J.W. Caldwell, P.A. Kollman, D.A. Case, Development and testing of a general amber force field, J. Comput. Chem. 25 (2004) 1157–1174.
[32] C. Lee,W. Yang, R.G. Parr, Development of the Colle-Salvetti correlation-energy formula into a functional of the electron density, Phys. Rev. B 37 (1988) 785.
[33] A.W.S. da Silva, W.F. Vranken, ACPYPE-antechamber python parser interface, BMC Research Notes 5 (2012) 367.
[34] S. Zheng, Q. Tang, J. He, S. Du, S. Xu, C.Wang, Y. Xu, F. Lin, VFFDT: a new software for preparing AMBER force field parameters for metal-containing molecular systems, J. Chem. Inf. Model. 56 (2016) 811–818.
[35] P. Mark, L. Nilsson, Structure and dynamics of the TIP3P, SPC, and SPC/E water models at 298 K, J. Phys. Chem. A 105 (2001) 9954–9960.
[36] W.L. Jorgensen, J. Chandrasekhar, J.D. Madura, R.W. Impey,M.L. Klein, Comparison of simple potential functions for simulating liquid water, J. Chem. Phys. 79 (1983) 926–935.
[37] M. Parrinello, A. Rahman, Polymorphic transitions in single crystals: a new molecular dynamics method, J. Appl. Phys. 52 (1981) 7182–7190.
[38] A. Rahman, F.H. Stillinger, Molecular dynamics study of liquid water, J. Chem. Phys.

55 (1971) 3336–3359.
[39] A. Lemak, N. Balabaev, On the Berendsen thermostat, Mol. Simul. 13 (1994) 177–187.
[40] T. Darden, D. York, L. Pedersen, Particlemesh Ewald: an N·log (N)method for Ewald sums in large systems, J. Chem. Phys. 98 (1993) 10089–10092.
[41] U. Essmann, L. Perera, M.L. Berkowitz, T. Darden, H. Lee, L.G. Pedersen, A smooth particle mesh Ewald method, J. Chem. Phys. 103 (1995) 8577–8593.
[42] H. Farrokhpour, H. Hadadzadeh, F. Darabi, F. Abyar, H.A. Rudbari, T. Ahmadi-Bagheri, A rare dihydroxo copper (II) complex with ciprofloxacin; a combined experimental and ONIOM computational study of the interaction of the complex with DNA and BSA, RSC Adv. 4 (2014) 35390–35404.
[43] M. Svensson, S. Humbel, R.D. Froese, T. Matsubara, S. Sieber, K. Morokuma, ONIOM: amultilayered integrated MO+MMmethod for geometry optimizations and single point energy predictions. A test for Diels−Alder reactions and Pt (P (t-Bu) 3) 2+ H2 oxidative addition, J. Phys. Chem. 100 (1996) 19357–19363.
[44] T. Vreven, K.S. Byun, I. Komáromi, S. Dapprich, J.A. Montgomery Jr., K. Morokuma, M.J. Frisch, Combining quantum mechanics methods with molecular mechanics methods in ONIOM, J. Chem. Theory Comput. 2 (2006) 815–826.
[45] P. Fromherz, B. Rieger, Photoinduced electron transfer in DNA matrix from intercalated ethidium to condensed methylviologen, J. Am. Chem. Soc. 108 (1986) 5361–5362.
[46] M.Waring, Complex formation between ethidium bromide and nucleic acids, J.Mol. Biol. 13 (1965) 269–282.
[47] M. Ganeshpandian, R. Loganathan, E. Suresh, A. Riyasdeen, M.A. Akbarsha, M. Palaniandavar, New ruthenium (II) arene complexes of anthracenyl-appended diazacycloalkanes: effect of ligand intercalation and hydrophobicity on DNA and protein binding and cleavage and cytotoxicity, Dalton Trans. 43 (2014) 1203–1219.
[48] E.M. Mrkalić, R.M. Jelić, O.R. Klisurić, Z.D.Matović, Synthesis of novel palladium (II) complexes with oxalic acid diamide derivatives and their interaction with nucleosides and proteins. Structural, solution, and computational study, Dalton Trans. 43 (2014) 15126–15137.

[49] Y.-Q.Wang, H.-M. Zhang, G.-C. Zhang,W.-H. Tao, S.-H. Tang, Interaction of the flavonoid hesperidin with bovine serum albumin: a fluorescence quenching study, J. Lumin. 126 (2007) 211–218.
[50] J.R. Lakowicz, Plasmonics in biology and plasmon-controlled fluorescence, Plasmonics 1 (2006) 5–33.
[51] S.U. Dighe, S. Khan, I. Soni, P. Jain, S. Shukla, R. Yadav, P. Sen, S.M. Meeran, S. Batra, Synthesis of β-carboline-based n-heterocyclic carbenes and their antiproliferative and antimetastatic activities against human breast cancer cells, J. Med. Chem. 58 (2015) 3485–3499.
[52] P.D. Ross, S. Subramanian, Thermodynamics of protein association reactions: forces contributing to stability, Biochemist 20 (1981) 3096–3102.
[53] M. Sirajuddin, S. Ali, A. Badshah, Drug–DNA interactions and their study by UV–visible, fluorescence spectroscopies and cyclic voltametry, J. Photochem. Photobiol. B 124 (2013) 1–19.
[54] K. Abdi, H. Hadadzadeh, M. Weil, H.A. Rudbari, Mono-and polynuclear copper (II)

complexes based on 2, 4, 6-tris (2-pyridyl)-1, 3, 5-triazine and its hydrolyzed form, Inorg. Chim. Acta 416 (2014) 109–121.
[55] S. Kathiresan, S. Mugesh, M. Murugan, F. Ahamed, J. Annaraj, Mixed-ligand copper (II)-phenolate complexes: structure and studies on DNA/protein binding profiles, DNA cleavage, molecular docking and cytotoxicity, RSC Adv. 6 (2016) 1810–1825.
[56] C. Ozluer, H.E.S. Kara, In vitro DNA binding studies of anticancer drug idarubicin using spectroscopic techniques, J. Photochem. Photobiol. B 138 (2014) 36–42.
[57] J.W. Lown, A.V. Joshua, Molecular mechanism of binding of pyrrolo (1, 4) benzodiazepine antitumour agents to deoxyribonucleic acid: anthramycin and tomaymycin, Biochem. Pharmacol. 28 (1979) 2017–2026.
[58] M. Kyropoulou, C.P. Raptopoulou, V. Psycharis, G. Psomas, Ni (II) complexes with non-steroidal anti-inflammatory drug diclofenac: structure and interaction with DNA and albumins, Polyhedron 61 (2013) 126–136.
[59] F. Zsila, Z. Bikadi, M. Simonyi, Probing the binding of the flavonoid, quercetin to human serum albumin by circular dichroism, electronic absorption spectroscopy and molecular modeling methods, Biochem. Pharmacol. 65 (2003) 447–456.
[60] V.I. Ivanov, L.E. Michenkova, A.K. Schyolkina, A.I. Poletayev, Different conformations of double-stranded nucleic acid in solution as revealed by circular dichroism, Biopolymers 12 (1973) 89–110.
[61] C. Li, J.-X. Wang, Y. Le, J.-F. Chen, Studies of bicalutamide–excipients interaction by combination of molecular docking and molecular dynamics simulation, Mol. Pharm. 10 (2013) 2362–2369.